Minireview

Critical assessment of a proposed model of Shaker

Muriel Lainé[a], Diane M. Papazian[b], Benoît Roux[c,*]

[a] Rockefeller University, 1280 York Ave, New York, NY 10021, USA
[b] Department of Physiology, David Geffen School of Medicine, University of California in Los Angeles, Los Angeles, CA 90095, USA
[c] Weill Medical College of Cornell University, 1300 York Ave, New York, NY 10021, USA

Received 21 December 2003; accepted 3 February 2004

First published online 18 March 2004

Edited by Fritz Winkler and Andreas Engel

Abstract Detailed three-dimensional structures at atomic resolution are essential to understand how voltage-activated K^+ channels function. The X-ray crystallographic structure of the KvAP channel has offered the first view at atomic resolution of the molecular architecture of a voltage-activated K^+ channel [Jiang et al. (2003) Nature 423, 33]. In the crystal, the voltage sensors are bound by monoclonal Fab fragments, which apparently induce a non-native conformation of the tetrameric channel. Thus, despite this significant advance our knowledge of the native conformation of a Kv channel in a membrane remains incomplete. Numerous results from different experimental approaches provide very specific constraints on the structure of K^+ channels in functional conformations. These results can be used to go further in trying to picture the native conformation of voltage-gated K^+ channels. However, the direct translation of all the available information into three-dimensional models is not straightforward and many questions about the structure of voltage-activated K^+ channels are still unanswered. Our aim in this review is to summarize the most important pieces of information currently available and to provide a critical assessment of the model of Shaker recently proposed by Lainé et al. [Neuron 39 (2003) 467].

Key words: Potassium channel; X-ray; Shaker

1. Introduction

Voltage-gated K^+ channels are transmembrane proteins that control and regulate the flow of K^+ ions across cell membranes. They activate in response to changes in membrane potential and are essential for the propagation of action potentials in excitable cells. The Shaker K^+ channel from *Drosophila melanogaster* [1] is one of the most studied voltage-activated K^+ channels. At the cell surface Shaker channels are tetramers [2], and each subunit consists of six transmembrane segments, S1–S6. The first four segments of each subunit, S1–S4, act as a 'voltage sensor', which detects the potential across the membrane and controls the gating of the channel [3–9]. The pore, which is responsible for rapid and selective ion conduction, is formed by the close association of the last two segments from each of the four subunits around a central axis. Electrophysiological [10–15], crystallographic [12,16,17] and computational studies [18–20] have helped elucidate the basic mechanism of K^+ permeation. The molecular conformations of the voltage sensor and how they are coupled to the central pore domain are less well understood.

Recently, a first view of the three-dimensional (3D) structure of a voltage-gated channel at atomic resolution was obtained using X-ray crystallography for the KvAP channel [21]. Two independent X-ray structures were obtained. The full tetrameric channel was crystallized in complex with a monoclonal Fab antibody fragment bound to the S3–S4 loop (Fig. 1A). In addition, the isolated voltage sensor, consisting of S1–S4, was also crystallized, again with a monoclonal Fab antibody bound to the S3–S4 loop. The conformations of the voltage sensor in the two X-ray structures are quite different. Furthermore, recognizing that the structure of the full channel was not entirely consistent with the expected architecture of the functional channel based on numerous experimental results, the authors concluded that the X-ray structure was probably distorted to some extent [21,22]. Thus, although these crystal structures have provided valuable information, our knowledge of the native conformation of a voltage-gated K^+ channel is incomplete. The occurrence of such a non-native conformation in protein crystallography appears to be highly unusual, but in this case may be due to the combined effect of the detergent and the interaction of the large, rigid Fab fragment with the highly flexible voltage sensor domain.

Additional experiments were performed to probe the movement of the voltage sensor in lipid membranes by tethering biotin to various positions and assessing whether avidin could access the biotin from either side of the membrane [23]. In addition, the significance of the distortion in the full-length channel structure was examined by docking the X-ray structure of the isolated voltage sensor (from the beginning of S2 to the end of S4) onto the central pore domain by superposing S2 (Fig. 1B); comparison with the full-length structure (Fig. 1A) led the authors to conclude that the crystallographic structure of the full-length channel was not very far from its membrane-bound conformation [22]. Models of the resting and activated functional states of the channel in its membrane environment were then developed accordingly, on the basis of the information from the X-ray structures and the biotin accessibility data [23]. A representation of the open state is shown in Fig. 1C.

In the KvAP structural models, it is proposed that the S4 segment is located at the periphery of the protein, where pos-

*Corresponding author. Fax: (1)-212-746 4843.
E-mail address: benoit.roux@med.cornell.edu (B. Roux).

0014-5793/04/$30.00 © 2004 Published by Elsevier B.V. on behalf of the Federation of European Biochemical Societies.
doi:10.1016/S0014-5793(04)00273-X

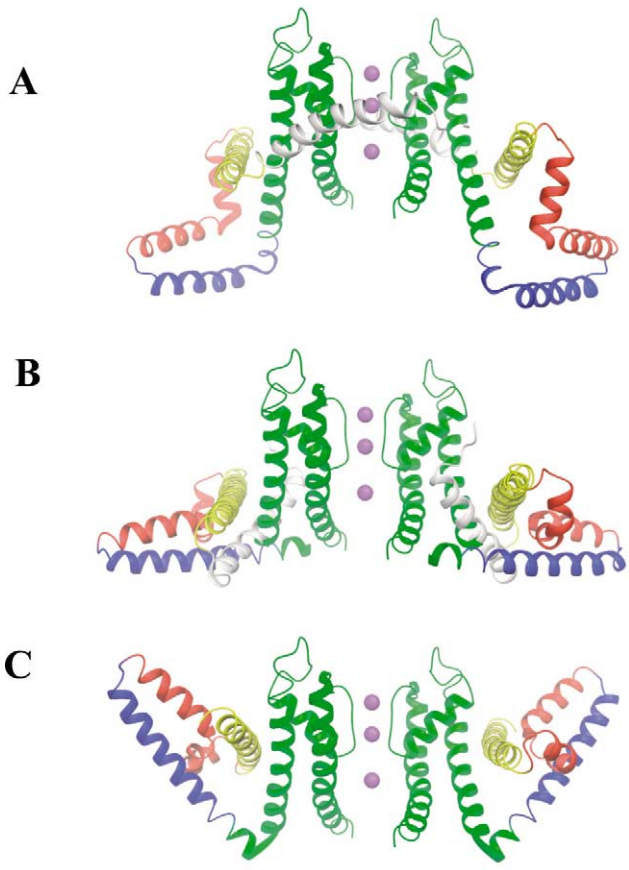

Fig. 1. Structures of the KvAP channel from Jiang et al. [21,23]; S1 (light blue), S2 (yellow), S3 (red), S4 (dark blue) and S5–S6 (green). Only two subunits are shown for the sake of clarity. A: X-ray structure of the full-length KvAP channel viewed from the side with the intracellular solution below [21]. B: Identical view with the X-ray structure of the isolated voltage sensor (S1–S4) docked according to the position of S2 in the X-ray structure of the full-length channel (obtained by superposing the backbone of S2 from the two X-ray structures) [21]. C: Representation of the modeled open state structure of KvAP based on the paddle depth and orientation [23].

itively charged S4 residues that sense changes in membrane potential are in contact with the hydrocarbon lipids while S2 lies close to the pore (Fig. 1C). The location of S4 was motivated by the observation that channels biotinylated along S4 appear to be able to drag biotin and its linker all the way across the membrane [23]. Nonetheless, such a structural feature departs considerably from most previous models of voltage-gated channels, which typically assumed that S4 is a transmembrane segment surrounded by other parts of the protein, and it is fair to say that there is a lack of consensus on this matter at the present time (for a review, see [24]).

One can try to go further by exploiting all the information that is available. A wide variety of experimental approaches including electrophysiology, biochemistry, site-directed mutagenesis, resonance energy transfer, and electron microscopy have also been used to probe the structure and function of voltage-gated K^+ channels. Undoubtedly, the large number of available experimental results put very specific constraints on the architecture of voltage-gated K^+ channels, although often indirectly. However, the 'translation' of all the available information into a 3D structure is not a straightforward (or risk-free!) exercise because it entails a critical assessment of the significance of experimental results obtained from widely different methods. Nonetheless, it is a worthwhile exercise because the resulting models provide a unified basis upon which the data from various sources can be compared and assessed. Our hope is that such models can play a useful role in the design of future experiments by indicating the areas of greatest uncertainty in the structure, and by helping to identify possible inconsistencies between the existing data.

The focus of the present paper is to regroup and review the available experimental data and to provide a critical assessment of a model of Shaker in the activated state that was recently proposed [25]. This model is shown in Fig. 2. In the model, the S1–S4 segments forming the voltage sensor domain are transmembrane α-helices. More specifically, the S4 segment is located near the groove formed at the interface between pore regions of adjacent subunits, nearly halfway between neighboring S5 helices. The assumption that the S1–S4 segments adopt a helical conformation is consistent with the X-ray structure of the KvAP channel [21]. Although the model shown in Fig. 2 differs markedly from the model proposed by Jiang et al. [23] (Fig. 1C), the organization of the voltage sensor is quite similar to that seen in the X-ray structure of the isolated voltage sensor domain of KvAP [21], with S1–S4 packed in a counterclockwise fashion when viewed from the extracellular side of the membrane [26]. Therefore, the general organization of S1–S4 in the model is consistent with part of the structural information from X-ray crystallography. In the following, we will review the most important experimental results upon which the Shaker model shown in

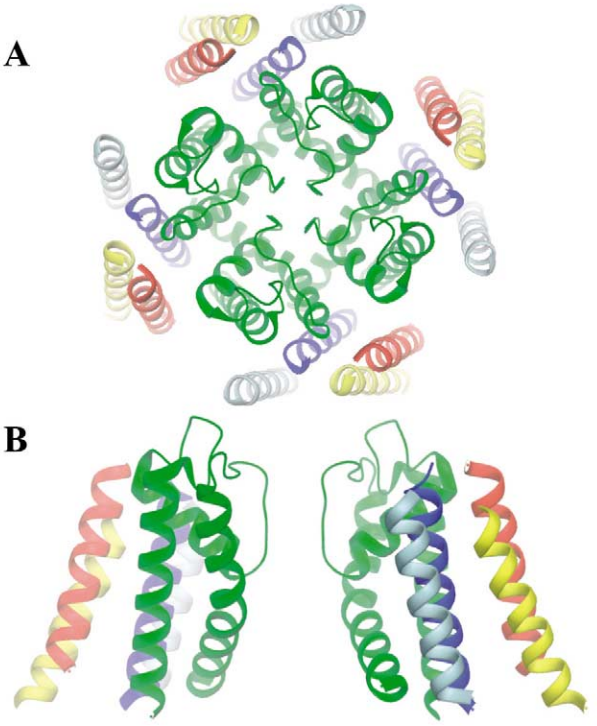

Fig. 2. Top (A) and side (B) view of the model of Shaker in the activated state proposed by [25]. S1 (light blue), S2 (yellow), S3 (red), S4 (dark blue) and S5–S6 (green). Only two subunits are shown in B for the sake of clarity.

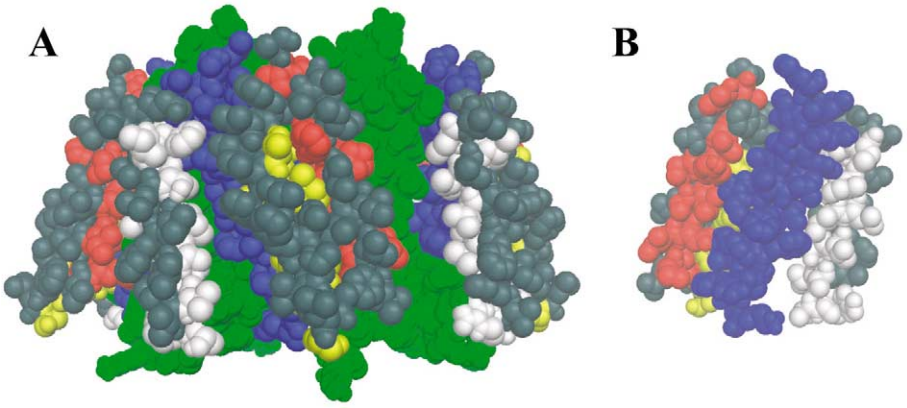

Fig. 3. Trp-tolerant positions of S1–S3 from the scanning studies of [27,28] are highlighted (dark gray). A side view from the lipid membrane (A) and a view of the voltage sensor S1–S4 seen from the pore (B) are shown. It is seen in B that no Trp-tolerant positions of S1–S3 are at the buried interface between the voltage sensor and the pore domain. S1 (white), S2 (yellow), S3 (red), S4 (blue) and S5–S6 (green).

Fig. 2 is based. The paper concludes with a brief discussion of the strengths and pitfalls of the current efforts.

2. Scanning mutagenesis of S1–S3

Miller and co-workers have performed site-directed substitution of all residues in S1–S3. Helical periodicity of functional alteration in the voltage–activation curves and gating kinetics was observed throughout S1 and S2. The function of the channel was significantly affected after Trp substitution at a number of positions [27,28]. However, channel function was not affected in many other positions. In the case of S3, the observations were similar but more complex. The distribution of Trp-tolerant positions was roughly consistent with a helical secondary structure for the amino-terminal end of S3, although the results were not as clear towards the carboxy-terminus [27]. Results from Ala [29] and Lys scanning [30] with the Kv2.1 (drk1) K^+ channel suggest that the S3 segment is entirely helical, but that the amino-terminal part interfaces with both lipid and protein, whereas the carboxy-terminal part interfaces with water. Interestingly, comparison of the amino acid sequence of several channels in the Kv family showed that the Trp-tolerant sites exhibit a high level of sequence variability, whereas the Trp-intolerant sites are highly conserved [27]. This observation further reinforces the suggestion that Trp-tolerant positions in the Shaker K^+ channel are exposed to the hydrocarbon region of the lipid bilayer [27,28], while the Trp-intolerant residues are involved in protein–protein contacts. As shown in Fig. 3, the Trp-tolerant positions are all clustered on a single face of the putative α-helical segments and are projecting towards the hydrocarbon region of the lipid bilayer in the model of Lainé et al. [25]. Remarkably, the break in S3, observed also in the X-ray structure of KvAP, had been previously deduced on the basis of scanning mutagenesis experiments [30,31]. Such a break in S3 was not incorporated in our model for simplicity.

3. Interactions between S2, S3 and S4

Many experimental studies have provided information on the relative position of the S1, S2, S3 and S4 segments. Using an intragenic suppression strategy, Tiwari-Woodruff et al. [32] showed that charge reversal mutations of E283 in S2 and K374 in S4 disrupt maturation of the protein. Maturation was specifically and efficiently rescued by second-site charge reversal mutations, strongly suggesting that electrostatic interactions exist between E283 in S2 and R368 and R371 in S4, and between K374 in S4, E293 in S2, and D316 in S3. Further investigation suggested that the interaction between E283 in S2 and R368 in S4 is likely to be important in an intermediate closed conformation along the activation pathway, whereas the interaction between E283 and R371 in S4 is probably important for the activated conformation of the voltage sensor [33]. In ether-à-go-go (eag), Tang et al. [34] showed that extracellular Mg^{2+} directly modulates the activation process by binding simultaneously to D278 in S2 (corresponding to I287 in Shaker) and D327 in S3 (corresponding to F324 in Shaker). Furthermore, evidence has been presented that the detailed molecular rearrangements that contribute to voltage-dependent activation in eag and Shaker channels are conserved, justifying the combination of constraints derived from these channels in one structural model [35]. As observed in Fig. 4, the identification of this additional pair of residues from eag constrains considerably the packing of the segments

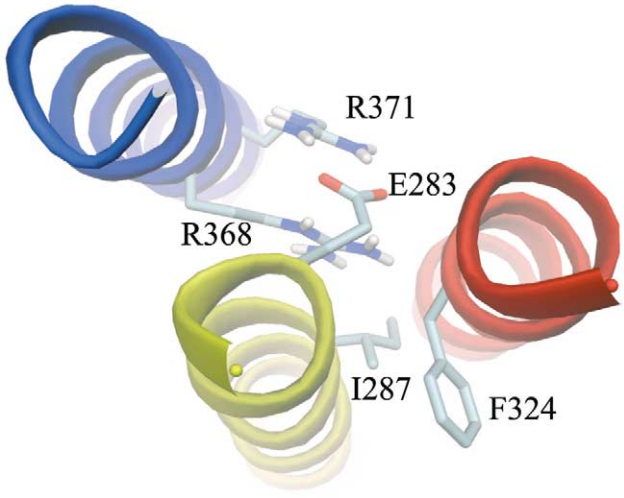

Fig. 4. Tertiary interactions that determine the relative packing of S2 (yellow), S3 (red) and S4 (blue). Based on [26,32–35].

S2–S4 in the voltage sensor of K^+ channels [26,34–36], leading to a unique arrangement of all the transmembrane segments except S1. Although no experimental data define its location relative to the other transmembrane segments, surveys of membrane proteins indicate that transmembrane helices generally pack against neighbors in the sequence [37]. This would suggest that S1 should be near S2, which is the arrangement observed in the structure of the isolated voltage sensor of KvAP [21].

4. Location of S4 relative to the pore

Cha et al. [38] used lanthanide-based resonance energy transfer (LRET) to measure distances between Shaker potassium channel subunits at specific residues. Specific sites in the channel were labelled by substituting a cysteine for particular residues and attaching a cysteine-reactive compound of either a donor (a terbium-chelate maleimide) or an acceptor (fluorescein maleimide). In particular, a distance of 45 Å between two V363 residues in S4 segments across the tetramer was estimated using this approach. As observed in Fig. 5, the S4 segment must be localized near the groove between adjacent subunits to satisfy this distance. Importantly, the estimated distances from LRET are completely consistent with the results from Blaustein et al. [39] who used a method based on tethered quaternary ammonium (QA) pore blockers. To localize the S1–S4 segments relative to the central pore, a series of compounds of varying length were tethered to specific test residues using site-directed cysteine mutations. By examining the probability of blockade as a function of the length of the compounds, it was shown that the extracellular ends of S1 and S3 are approximately 30 Å from the external opening of the pore while the S3–S4 linker is located at 17–18 Å from the pore.

The atomic proximity of S4 to S5 was also revealed via the

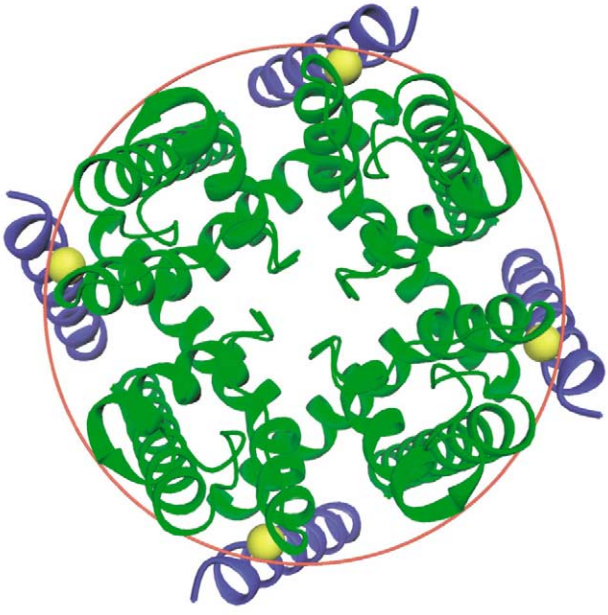

Fig. 5. Circle of 45 Å diameter corresponding to the distance between V363 (Cβ shown in yellow) residues located in S4 segments in opposite subunits across the pore axis as estimated by LRET [38].

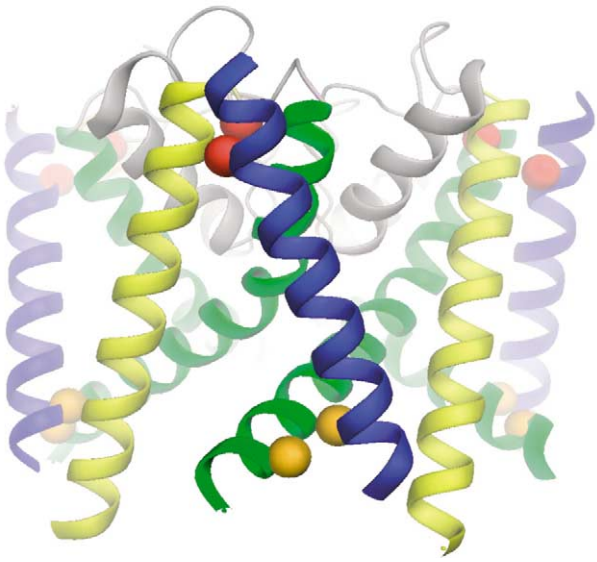

Fig. 6. Location of S4 at the interface between adjacent subunits from [25]. The S4 segment (in blue) and the central pore domain formed by S5 (yellow) and S6 (green) are shown. The red spheres represent the Cβ atoms of R362 and A419 [25], and the orange spheres represent the Cβ atoms of R377 and Y483 corresponding to the position of D540 and R665 in the HERG channel [48].

spontaneous formation of intersubunit disulfide bonds between R362 and F416 and between R362 and A419 when cysteines were introduced at these positions [25]. Circular tetramers of Shaker subunits were specifically observed by sodium dodecyl sulfate–polyacrylamide gel electrophoresis when these residues were substituted by cysteine, indicating that the contacts occurred between residues in adjacent subunits. In contrast the corresponding single cysteine mutants or other double cysteine mutants in this same region did not form disulfide-bonded tetramers. Furthermore, after reduction of the disulfide bonds, the cysteines in the double mutant 362C+419C formed a high affinity Cd^{2+} binding site ($[Cd^{2+}]_{0.5} \approx 190$ nM) that stabilized the Shaker channel in an activated conformation. Reduced R362C+F416C channels also bound Cd^{2+} with high affinity. Similarly, a high affinity Zn^{2+} binding site ($\sim$400 nM) was formed when R362 and A419 were substituted by His. Of particular importance, the measured affinities are comparable to those measured in experiments involving an engineered binding site with two (instead of three) His residues in the active site of human carbonic anhydrase II [40], suggesting that no significant structural distortions of the channel are induced by the metal bridge introduced between S4 and the pore domain. It was confirmed that the contacts involved residues from two different subunits by electrophysiological characterization of co-injected single mutants (R362H and A419H). Formation of similar disulfide bonds between pairs of cysteine residues introduced at position 416 and at variable positions in the S3–S4 linker confirmed the proximity of S4 in relation to the pore domain [41,42].

These experimental results place S4 in proximity with the pore domain near the groove that is formed at the boundaries of two subunits. The location of S4 in the model is depicted in Figs. 6 and 7. The carboxy-terminus of the S4 segment from one subunit makes contact with the neighboring subunit in the

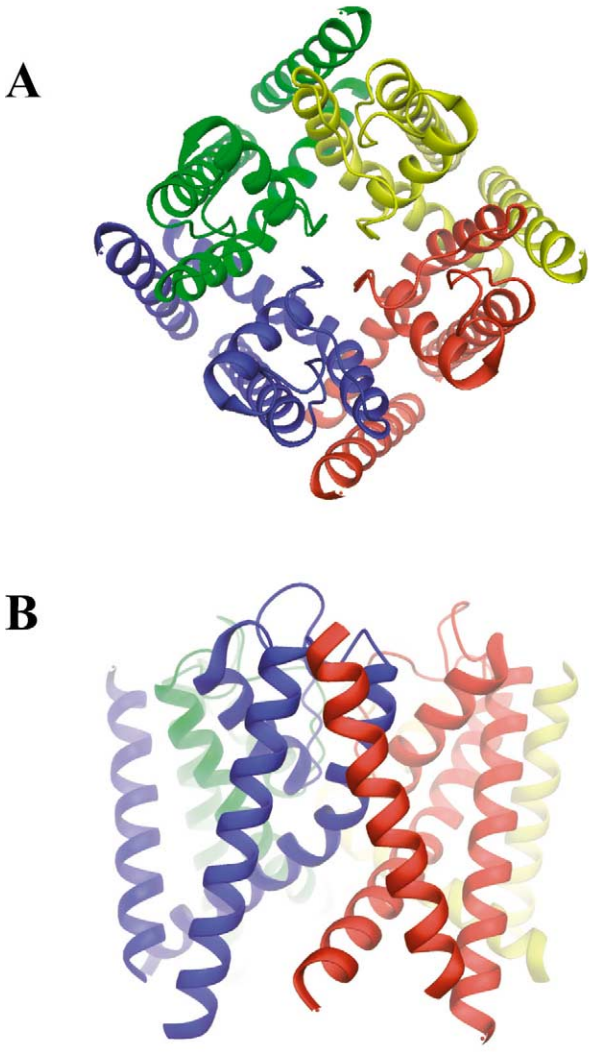

Fig. 7. Top (A) and side (B) view of Shaker showing how the carboxy-terminus of S4 from one monomer makes contact with S5 of the neighboring subunit in the clockwise direction as seen from the extracellular side. Based on [25]. Each subunit is shown as a different color.

clockwise direction when seen from the extracellular side of the membrane. Interestingly, scanning mutagenesis of the Shaker pore domain identified a number of residues with large effects on channel gating that map directly under the position of S4 in the model [43]. Residues that mapped to the 'surface' of the central pore domain based on the X-ray structure of KcsA were mutated. Mutations that significantly shifted the gating charge–voltage relationship were found to cluster near the interface between adjacent pore domain subunits, suggesting that this is one region where the voltage sensor contacts the pore. The residues displaying the largest perturbations in channel gating are highlighted in Fig. 8.

5. Accessibility measurements

Gandhi et al. [41] examined the solvent accessibility of residues from S1 through S3. Cysteine residues were introduced at specific positions in S1–S3 and labeled with tetramethylrhodamine maleimide, a fluorescent molecule, to probe the accessibility of those positions. Since this reagent is known to be membrane-impermeable, any voltage-dependent changes in fluorescence relative to the wild-type channel are indicative that the position is accessible from the external solution. The most important fluorescent changes were observed at the C-terminal side of S1 (residues 246–254), the N-terminal side of S2 (residues 274–280) and the C-terminal side of S3 (part of S3b, residues 330–340). No significant change in fluorescence was observed from residues 235 to 246 in S1, or residues 281 to 329 in S2–S3. These results show that each helix has an extremity that is exposed to the external solution.

Starace et al. [44,45] used histidine scanning mutagenesis of the S4 segment to address the state-dependent accessibility of S4 residues from the external or internal side of the membrane. Histidine mutations introduced minimal interference of voltage sensor motion and therefore their titration provided extensive information regarding charge movement of the voltage sensor across the membrane. In the presence of a pH gradient histidine introduced at position R365, R368, or R371 showed that each of these residues traverses entirely from internal exposure at hyperpolarized potentials to external exposure at depolarized potentials. The most remarkable result from these experiments is the observation that substitution of Arg at position 371 by a histidine transforms the voltage sensor into a proton-conducting pore at depolarized membrane potentials.

Voltage-dependent changes in the sidedness of exposure have also been observed for S4 residues in KvAP. Site-specific biotinylation of the KvAP channel and inhibition by avidin was used to probe the accessibility of the S3–S4 loop [23]. The results indicated that residues from G101 (corresponding to position F324 in Shaker) to L122 (corresponding to V367 in Shaker) were accessible from the extracellular side of the membrane when the channel is in the activated state [23]. Two positions, L121 and L122, located near the center of S4 were also accessible from the internal side when the channel is in the resting state.

These experimental results are highlighted in Fig. 9 using our model of Shaker in the activated state. The idea that the S1–S4 helices span the membrane appears to be consistent

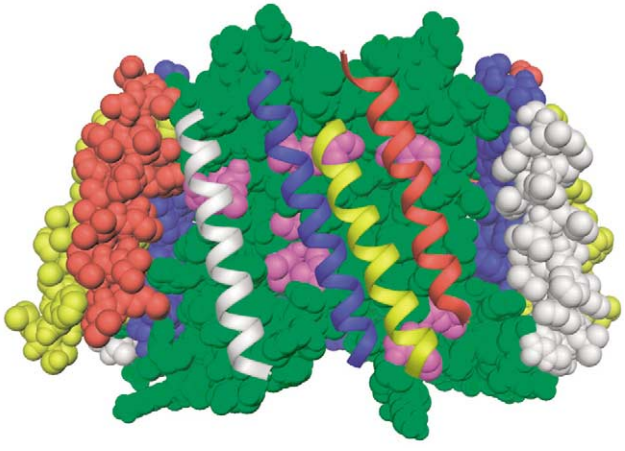

Fig. 8. Residues at the surface of the pore domain formed by S5–S6 (green) shown by site-directed mutagenesis to significantly affect the gating charge–voltage relationship of Shaker [43] are highlighted in magenta (R394, L398, V408, L409, F433, I457, V458, A465, L468, I477). S1 (white), S2 (yellow), S3 (red) and S4 (blue) are also shown.

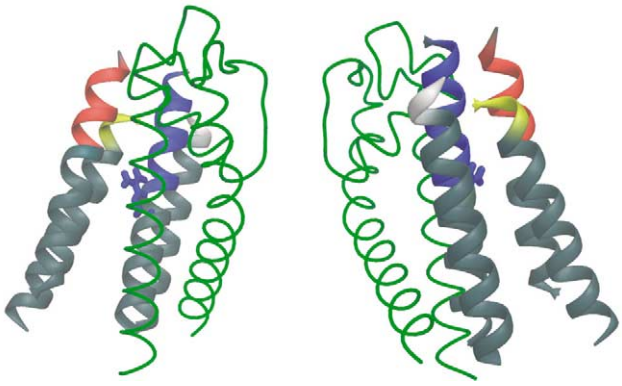

Fig. 9. Side view of Shaker highlighting the residues of S1 (white), S2 (yellow), S3 (red) and S4 (blue) that are accessible from the external side based on the data from [23,41]. The inaccessible residues are shown in dark gray. The pore domain S5–S6 is depicted as a thin wire (green). The residue R371 of S4, which confers a proton conductance to Shaker in the activated state when substituted by a His, is depicted in sticks [44,45].

with all available accessibility measurements for the activated state. Furthermore, the Arg at position 371, which yields a proton-conducting pore in the activated state when substituted by a histidine, is located near the middle of the membrane, between S3 and S4. It is conceivable that this configuration could constitute a passage for proton flux.

6. Concluding discussion

Experimental evidence from a wide variety of indirect approaches constrains the structural organization of voltage-dependent K^+ channels in the native, functional state. Although the evidence is indirect, data sets obtained from different approaches are strikingly compatible, resulting in an approximate model for the structure of the channel that is quite different from the KvAP X-ray structure and the proposed models (see Fig. 1). Given the limited amount of information presently available, any structural model of a voltage-gated K^+ channel is necessarily 'low-resolution'. The purpose of such structural models must be, therefore, to delineate and clarify, as objectively as possible, the current state of knowledge about K^+ channels. Our hope is that such models can play a useful role in the design of future experiments.

The difficulties in attempting to deduce a structural model from indirect experimental data are illustrated by the case of the lactose permease of *Escherichia coli* (LacY), for which a crystallographic X-ray structure has recently been obtained [46]. Functionally, LacY can adopt two main conformations, 'inward-facing' or 'outward-facing', and the crystal structure clearly represents the inward-facing conformation. For years, this membrane transporter resisted efforts at crystallization and structural models were constructed using spatial constraints deduced indirectly from a multitude of experimental approaches including thiol cross-linking studies [47]. In retrospect, it appears that most of the previously deduced spatial restraints were indeed meaningful, although they cannot be all satisfied simultaneously since they correspond to a mixture of the two conformational states of LacY. Therefore, an important lesson from LacY is that the functional state for which such spatial constraints are relevant must be identified as clearly and unambiguously as possible. From this point of view, one advantage of studying K^+ channels is the possibility to control the functional state of the channel via the transmembrane potential.

The current model places S4 near the groove between adjacent subunits. This position differs considerably from the models proposed by Jiang et al. [23] who placed S4 at the periphery of the protein, in contact with the hydrocarbon lipids (see Fig. 1). Nevertheless, the results from LRET (Fig. 5) [38], the tethered QA pore blockers [39], the engineered intersubunit disulfide bonds and metal bridges between S4 and the pore domain [25,41,42] all indicate that S4 is located in proximity to the central pore domain. Despite the fact that many of these experiments are burdened by intrinsic limitations, the evidence indicating the general location of S4 in the activated state seems compelling. The proposed model of Shaker in the activated state (Fig. 2) appears to be completely consistent with all the available functional data. This includes the position of the Trp-tolerant residues in S1–S3 (Fig. 3), the pairs of residues involved in likely tertiary interactions in S2–S4 (Fig. 4), the formation of an intersubunit contact between S4 and S5 (Fig. 6), the residues in S5–S6 affecting gating (Fig. 8), and the patterns of accessibility of S1–S4 (Fig. 9). Finally, examination of the model shown in Fig. 2 reveals that S4 can be exposed to the lipids, at least in part, leaving sufficient space to drag biotin and its long linker across the membrane (see also Fig. 3).

One of the most ad hoc assumptions in modeling Kv channels, prior to the KvAP crystallographic X-ray structures, was that the transmembrane segments S1–S4 adopted an α-helical conformation. Indeed, these segments are α-helices in both the X-ray structure of the complete channel and the X-ray structure of isolated voltage sensor [21]. This observation strengthens considerably the hypothesis that S1 and S4 are α-helices (though S3 has clearly more complexity). Nonetheless, such helical conformations are not an absolute and must be viewed critically. In particular, it should be emphasized that information concerning the resting (closed) state remains scarce and insufficient to construct a unique model. More information about both the active and the resting states of the channel will be essential to elucidate the mechanism of voltage gating.

7. Note added in proof

Recent results from single particle electron microscopy reconstruction with the KvAP channel suggest that S4 is located near the pore domain, in a configuration that appears to be compatible with the model shown in Figs. 5 and 6 (Q.-X. Jiang and R. MacKinnon, 118-Plat, Biophysical Society Meeting, Baltimore, MD, 2004).

Acknowledgements: This work was supported by grants form the National Institute of Health to D.M.P. (GM43459) and B.R. (GM62342). We are grateful to Francisco Bezanilla and Kenton Swartz for helpful discussions.

References

[1] Tempel, B.L., Papazian, D.M., Schwarz, T.L., Jan, Y.N. and Jan, L.Y. (1987) Science 237, 770–775.
[2] MacKinnon, R. (1991) Nature 350, 232–235.
[3] Papazian, D.M., Timpe, L.C., Jan, Y.N. and Jan, L.Y. (1991) Nature 349, 305–310.
[4] Liman, E.R., Hess, P., Weaver, F. and Koren, G. (1991) Nature 353, 752–756.

[5] Logothetis, D.E., Movahedi, S., Satler, C., Lindpaintner, K. and Nadal-Ginard, B. (1992) Neuron 8, 531–540.
[6] Aggarwal, S.K. and MacKinnon, R. (1996) Neuron 16, 1169–1177.
[7] Seoh, S.A., Sigg, D., Papazian, D.M. and Bezanilla, F. (1996) Neuron 16, 1159–1167.
[8] Bezanilla, F. (2000) Physiol. Rev. 80, 555–592.
[9] Yellen, G. (1998) Q. Rev. Biophys. 31, 239–295.
[10] Hodgkin, A.L. and Keynes, R.D. (1955) J. Physiol. 128, 61–88.
[11] Hille, B. and Schwarz, W. (1978) J. Gen. Physiol. 72, 409–442.
[12] Morais-Cabral, J.H., Zhou, Y. and MacKinnon, R. (2001) Nature 414, 37–42.
[13] Neyton, J. and Miller, C. (1988) J. Gen. Physiol. 92, 569–586.
[14] Neyton, J. and Miller, C. (1988) J. Gen. Physiol. 92, 549–567.
[15] Zhou, Y. and MacKinnon, R. (2003) J. Mol. Biol. 333, 965–975.
[16] Doyle, D.A., Morais Cabral, J., Pfuetzner, R.A., Kuo, A., Gulbis, J.M., Cohen, S.L., Chait, B.T. and MacKinnon, R. (1998) Science 280, 69–77.
[17] Zhou, Y., Morais-Cabral, J.H., Kaufman, A. and MacKinnon, R. (2001) Nature 414, 43–48.
[18] Bernèche, S. and Roux, B. (2001) Nature 414, 73–77.
[19] Bernèche, S. and Roux, B. (2003) Proc. Natl. Acad. Sci. USA 100, 8644–8648.
[20] Aqvist, J. and Luzhkov, V. (2000) Nature 404, 881–884.
[21] Jiang, Y., Lee, A., Chen, J., Ruta, V., Cadene, M., Chait, B.T. and MacKinnon, R. (2003) Nature 423, 33–41.
[22] MacKinnon, R. (2003) FEBS Lett. 555, 62–65.
[23] Jiang, Y., Ruta, V., Chen, J., Lee, A. and MacKinnon, R. (2003) Nature 423, 42–48.
[24] Cohen, B.E., Grabe, M. and Jan, L.Y. (2003) Neuron 39, 395–400.
[25] Laine, M., Lin, M.C., Bannister, J.P., Silverman, W.R., Mock, A.F., Roux, B. and Papazian, D.M. (2003) Neuron 39, 467–481.
[26] Silverman, W.R., Roux, B. and Papazian, D.M. (2003) Proc. Natl. Acad. Sci. USA 100, 2935–2940.
[27] Hong, K.H. and Miller, C. (2000) J. Gen. Physiol. 115, 51–58.
[28] Monks, S.A., Needleman, D.J. and Miller, C. (1999) J. Gen. Physiol. 113, 415–423.
[29] Li-Smerin, Y. and Swartz, K.J. (2000) J. Gen. Physiol. 115, 673–684.
[30] Li-Smerin, Y. and Swartz, K.J. (2001) J. Gen. Physiol. 117, 205–218.
[31] Nguyen, T.P. and Horn, R. (2002) J. Gen. Physiol. 120, 419–436.
[32] Tiwari-Woodruff, S.K., Schulteis, C.T., Mock, A.F. and Papazian, D.M. (1997) Biophys. J. 72, 1489–1500.
[33] Tiwari-Woodruff, S.K., Lin, M.A., Schulteis, C.T. and Papazian, D.M. (2000) J. Gen. Physiol. 115, 123–138.
[34] Tang, C.Y., Bezanilla, F. and Papazian, D.M. (2000) J. Gen. Physiol. 115, 319–338.
[35] Silverman, W.R., Tang, C.Y., Mock, A.F., Huh, K.B. and Papazian, D.M. (2000) J. Gen. Physiol. 116, 663–678.
[36] Papazian, D.M., Silverman, W.R., Lin, M.C., Tiwari-Woodruff, S.K. and Tang, C.Y. (2002) Novartis Found. Symp. 245, 178–190; discussion 190–192, 261–264.
[37] Bowie, J.U. (1997) J. Mol. Biol. 272, 780–789.
[38] Cha, A., Snyder, G.E., Selvin, P.R. and Bezanilla, F. (1999) Nature 402, 809–813.
[39] Blaustein, R.O., Cole, P.A., Williams, C. and Miller, C. (2000) Nat. Struct. Biol. 7, 309–311.
[40] Kiefer, L.L. and Fierke, C.A. (1994) Biochemistry 33, 15233–15240.
[41] Gandhi, C.S., Clark, E., Loots, E., Pralle, A. and Isacoff, E.Y. (2003) Neuron 40, 515–525.
[42] Broomand, A., Mannikko, R., Larsson, H.P. and Elinder, F. (2003) J. Gen. Physiol. 122, 741–748.
[43] Li-Smerin, Y., Hackos, D.H. and Swartz, K.J. (2000) J. Gen. Physiol. 115, 33–50.
[44] Starace, D.M., Stefani, E. and Bezanilla, F. (1997) Neuron 19, 1319–1327.
[45] Starace, D.M. and Bezanilla, F. (2001) J. Gen. Physiol. 117, 469–490.
[46] Abramson, J., Smirnova, I., Kasho, V., Verner, G., Kaback, H.R. and Iwata, S. (2003) Science 301, 610–615.
[47] Sorgen, P.L., Hu, Y., Guan, L., Kaback, H.R. and Girvin, M.E. (2002) Proc. Natl. Acad. Sci. USA 99, 14037–14040.
[48] Tristani-Firouzi, M., Chen, J. and Sanguinetti, M.C. (2002) J. Biol. Chem. 277, 18994–19000.